2010-01-01

Silver Nanoparticle Polymer Composite Based Humidity Sensor

Aoife Power
Dublin Institute of Technology, aoife.power@dit.ie

Tony Betts
Dublin Institute of Technology, anthony.betts@dit.ie

John Cassidy
Dublin Institute of Technology, john.cassidy@dit.ie

Recommended Citation
Power, A., Betts, A. & Cassidy, J. (2010) Silver Nanoparticle Polymer Composite Based Humidity Sensor. *Analyst* vol.135, pp.1645 - 1652. doi:10.1039/c0an00133c

Silver Nanoparticle Polymer Composite based Humidity Sensor.

Aoife C. Power [a., c.], Anthony J. Betts [b., c.] and John F. Cassidy [a., c.]

[a] School of Chemical and Pharmaceutical Sciences, Dublin Institute of Technology, Kevin St., Dublin 8, Ireland.

[b] Directorate of Research & Enterprise, Dublin Institute of Technology, 143-149 Rathmines Rd., Dublin 6, Ireland.

[c] Applied Electrochemistry Group, Focas Institute, Dublin Institute of Technology, Camden Row Dublin 8, Ireland.

Silver nanoparticles were synthesised by a chemical reduction process in order to produce an aqueous colloidal dispersion. The resulting colloids were then characterised by a combination of UV-Vis spectroscopy, dynamic light scattering, X-Ray diffraction and transmission electron microscopy and the nanoparticles were found to have an average diameter of 20-22nm. The Ag/polymer nanocomposites were then applied to platinum interdigital electrodes as sensor coatings and the capability of the resulting sensor as a humidity detector investigated. With the application of 1V, a current developed which was found to be directly proportional to humidity levels. The sensor gives a reversible, selective and rapid response which is proportional to levels of humidity within the range of 10% RH to 60% RH. An investigation into the mechanism of the sensor's response was conducted and the response was found to correlate well with a second order Langmuir adsorption model.

Introduction

Relative Humidity (RH) detection and its control are important in a wide range of industrial applications including the pharmaceutical, food and electronics industries. The close monitoring of RH during processes can help maintain product quality and can also be necessary during transport of materials [1–3].

Some humidity sensors have been developed based on a reversible interaction between a polymer and water vapour, hence acting as a gas sensor [4-5]. Existing humidity sensing methodologies also rely upon optical, gravimetric, capacitive, resistive, piezoresistive, and magnetoelastic properties of selected materials [6].

Nanomaterials were found to have significant roles in a diverse range of analytical methods particularly in sensing applications [7-11]. The increased interest in

nanomaterials, especially metallic nanostructures, may be attributed to the often novel physical and chemical properties these nanoparticles display when compared to their bulk counterparts [10, 12]. Previously, polymers have been widely utilized in a wide range of sensing devices with definite roles, either in the sensing mechanism or through immobilizing the species responsible for sensing of the analyte component. This is possible as polymers may be tailored for particular properties [13, 14], are easily processed, and may be selected to be inert in the environment containing the analyte. Coupling nanoparticles with specific polymers to form nanocomposites has been shown to be very effective in producing highly selective and sensitive gas sensors [15-18].

RH is generally measured and controlled by meters that detect change in a physical property of a thin film, such as capacitance, resistivity, or thermal conductivity. Often these control systems are relatively complex and expensive [19]. In this work the sensor is based on a polyvinyl alcohol (PVA) silver nanoparticle composite cast on an interdigital electrode array. On application of a constant potential (1V), a current develops which is proportional to levels of humidity from 10% to 60%. The response is reversible and fast at room temperature and it displays a high selectivity.

The intention of this work was to prepare and characterise a Ag/polymer nanocomposites and then investigate the composite materials performance as a sensor (with emphasis on the materials efficacy as a humidity sensor) when coated on an interdigital electrode array.

Experimental

Silver nitrate (purum p.a. > 99.0%), sodium borohydride (reagent Plus 99%) polyvinyl alcohol (PVA), (99+% hydrolyzed, typical M.W. 89000-98000 $gmol^{-1}$), acetonitrile (anhydrous, 99.8%), cyclohexane (anhydrous, 99.5%), ethanol (anhydrous, ≥ 99.5%) and methanol (anhydrous 99.8%), calcium nitrate tetrahydrate (> 99.0%), calcium chloride dehydrate (≥ 99.0%), and potassium acetate (98%) were all purchased from Sigma Aldrich and used as received without further purification with the exception of the solvents which were dried as per the methods outlined in Perrin [20].

The experimental process in this study comprised of a number of distinct steps. Firstly the preparation and characterisation of the nanocomposite colloids was performed,

followed by the optimisation of this preparation method. The Ag/polymer nanocomposite was cast on an interdigital array for use as a humidity sensor.

Initially silver nanoparticles were synthesised by a chemical reduction of $AgNO_3$ by $NaBH_4$ in an aqueous media [21-23] with PVA utilised as the capping (stabilising) agent. The role of PVA as a successful capping agent is well documented [24-27]. It was also observed that without the presence of the PVA, the stability of the colloids was drastically reduced with metallic silver formed due to aggregation of nanoparticles. PVA has been widely used for polymer nanocomposites due to its water solubility making the preparation virtually non-toxic [28] In this study the silver polymer content ratio was maintained at 1 mole of silver to every 1 mole of the PVA monomer .

It was necessary to optimise the preparation method as the ratio between Ag^+ and BH_4^- in the literature seemed to be unclear and usually BH_4^- was added in great excess [24-28]. There is a competing reduction of water by BH_4^- and it was felt useful to determine the stoichiometry of the reaction; Job's method was used for this purpose.

The sensor coatings were produced by casting the colloid Ag/polymer composites on platinum interdigital electrodes (CC2.W2), or graphite interdigital electrodes (CC1.W4), which were purchased from BVT Technologies and used as received (figure 1). A set volume, (0.1 ml), of the colloid was deposited by drop coating on to the surface of the electrodes and air dried over a period of 12 – 15 hours. Coating thickness was measured using a Reichert-Jung optical microscope.

The behaviour of the resulting coating as a humidity sensor was investigated as follows; a constant potential of 1V was then applied across the interdigital electrode using a Thompson ministat potentiostat and the resulting response measured. The sensor's response is a voltage signal which is produced across the 1kΩ 'counting' resistor on the potentiostat. The sensing membrane's responses to selected vapours were collected using a high-resolution data logger (PICO ADC 16).

All experiments were conducted at room temperature (20 ± 2^oC) and N_2 (Oxygen Free 99.998%, BOC Gases) was used as the reference gas. These vapour streams were produced by bubbling dry N_2 gas using a bubbler apparatus, as shown in Figure 2.

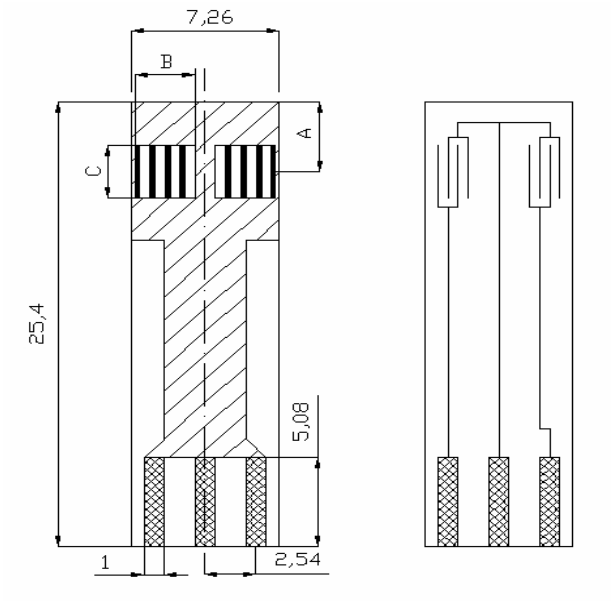

Figure 1. Schematic of BVT Technologies CC2.W* (*) conductometric sensor substrates, A= 4.00 ± 0.05 mm, B & C = 3.00 ± 0.05 mm. [29]

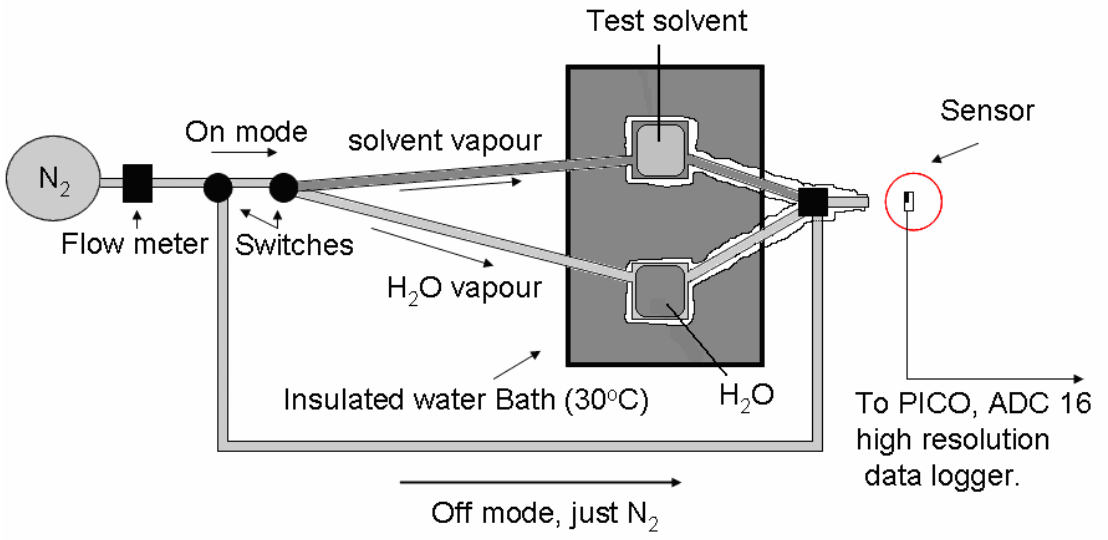

Figure 2. Bubbler apparatus schematic, the Dreschel flasks typically held a volume of 40 cm^3.

The sensitivity of the films response and suitability as a humidity sensor was further investigated by exposure of the sensor to a series of selected known humidity levels. A controlled environment chamber with humidity control system (Electro-Tech systems model 503-20) was used to set each humidity level. The relative humidity within the chamber was maintained at a set level in the range of 10 - 100% RH ± 1% RH. In addition the temperature of the environment was kept constant at 21.3 ± 0.1 °C.

Characterisation of the silver nanoparticles involved several techniques including; UV-Vis, dynamic light scattering (DLS) and X-Ray diffraction (XRD) analysis which were conducted using a Perkin Elmer, Lambda 900 Spectrometer, a Malvern, nano series Zetasizer and a Siemens Diffractometer, Model D500 respectively, Transmission Electron Microscope (TEM) images were captured with a JEOL, 100CX Transmission Electron Microscope.

Results and discussion

Colloid characterisation.

UV-Vis analysis.

The absorption spectrum of the colloid, shown in Figure 3, indicates the production of the nanoparticles where the presence of a plasmon absorption band at ~ 400 nm is characteristic of silver nanoparticles [30].

Such plasmon bands are a result of the unique physical properties of the nanoparticles themselves. When an external electro-magnetic field such as light is applied to a metal, the conduction electrons move collectively so as to screen the perturbed charge distribution in what is known as plasma oscillation. The Surface Plasmon Resonance (SPR) is therefore a collective excitation mode of the plasma localized near the metal surface. In the case of a metal nanoparticle, the surface plasmon mode is 'restricted' due to the small dimensions to which the electrons are confined, i.e. the surface plasmon mode must conform to the boundaries of the dimensions of the nanoparticle [27]. Therefore the resonance frequency of the surface plasmon oscillation of the metal nanoparticle is different from the plasma frequency of the bulk metal. Surface interactions can alter the optical properties and influence the spectral profile of the light scattered by the SPR of the metal nanoparticles. This feature can be employed as an indicator in sensing interactions. Among the metal nanoparticles known to exhibit SPR, silver nanoparticles have an especially strong SPR. Particle size may be determined using Mie theory which solves Maxwell's equations [32] which in turn

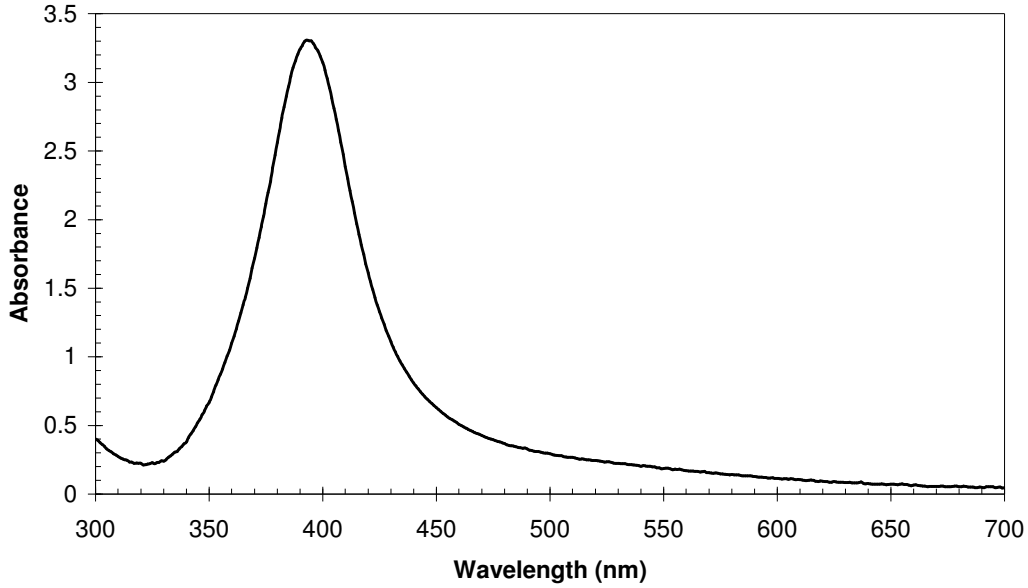

Figure 3. UV-Vis spectrum of stable aqueous colloidal Ag polymer mixture, with λ max of 391 nm. $[Ag^+]$ = 1M (0.5cm^3), [PVA] = 1% wt/wt (0.66 cm^3), $[NaBH_4]$ = 0.1M (6cm^3) diluted to 10cm^3 and maintained at a low temperature.

describe the extinction spectra (extinction = scattering + absorption) of spherical particles of arbitrary size. The spectrum illustrated in Figure 3 displays the characteristic SPR of silver nanoparticles, commonly seen in the literature [31, 33, 34].

Jobs Method.

The stoichiometric ratio of Ag^+ to BH_4^- in the PVA stabilised colloids was determined using Jobs method [35]. A series of solutions was prepared, each containing the same total number of moles of Ag^+ and BH_4^-, but utilising different ratios. The solution with the maximum amount of product, (nanoparticles) yields the stoichiometric ratio [31]. The maximum absorbance at 400nm for the range of solutions prepared was observed in the solution which corresponded to a ratio of 1:1 for Ag^+ and BH_4^-. Therefore the overall equation resulting in the production of silver nanoparticles is therefore proposed to be.

$$\mathbf{AgNO_3 + NaBH_4 \rightarrow Ag^0 + \tfrac{1}{2}\, H_2 + \tfrac{1}{2}\, B_2H_6 + NaNO_3} \qquad \mathbf{(1)}$$

Dynamic light scattering, DLS.

DLS, shown in Figure 4, confirmed the production of particles ranging in size between about 8nm – 38nm, with an average diameter of 21-22nm.

Size analysis by DLS utilises the Brownian motion that particles, emulsions and molecules in suspension undergo as a result of bombardment by solvent molecules. If the particles are illuminated with a laser, the intensity of the scattered light fluctuates at a rate that is dependent upon the size of the particles as smaller particles are "hit" more frequently by the solvent molecules and move more rapidly. Analysis of these intensity fluctuations yields the velocity of the Brownian motion and hence the particle size using the Stokes-Einstein relationship [36].

$$\mathbf{D = k_B T / 6\pi\eta r} \qquad \mathbf{(2)}$$

Where D is the diffusion constant (m^2s^{-1}), k_B is Boltzmann's constant (JK^{-1}), T is the absolute temperature (K), η is the viscosity of the solvent ($kgm^{-1}s^{-1}$) and r is the particle radius (m).

Transmission electron microscopy.

Using TEM, an image of the nanoparticles, (Figure 5) was obtained arising from the interaction of the coating and the beam of electrons transmitted through the coating. Before analysis, the colloidal sample (prepared in the same manner as Figure 2) was diluted in methanol and sonicated for 30 mins, before being cast onto the TEM grid (Agar scientific, formvar/carbon 200 mesh (Cu)) by drop coating. The average

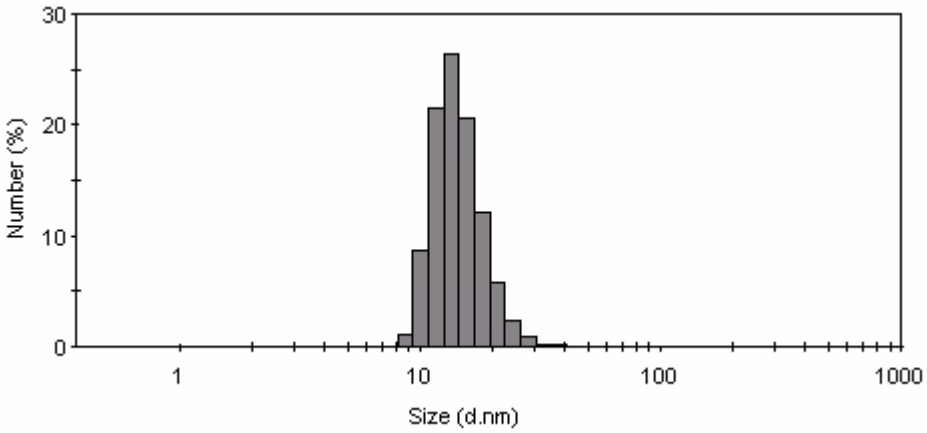

Figure 4. Distribution of particle diameters within the Ag PVA colloid determined by DLS. The sample analysised was prepared in an identical manner to that in Figure 1.

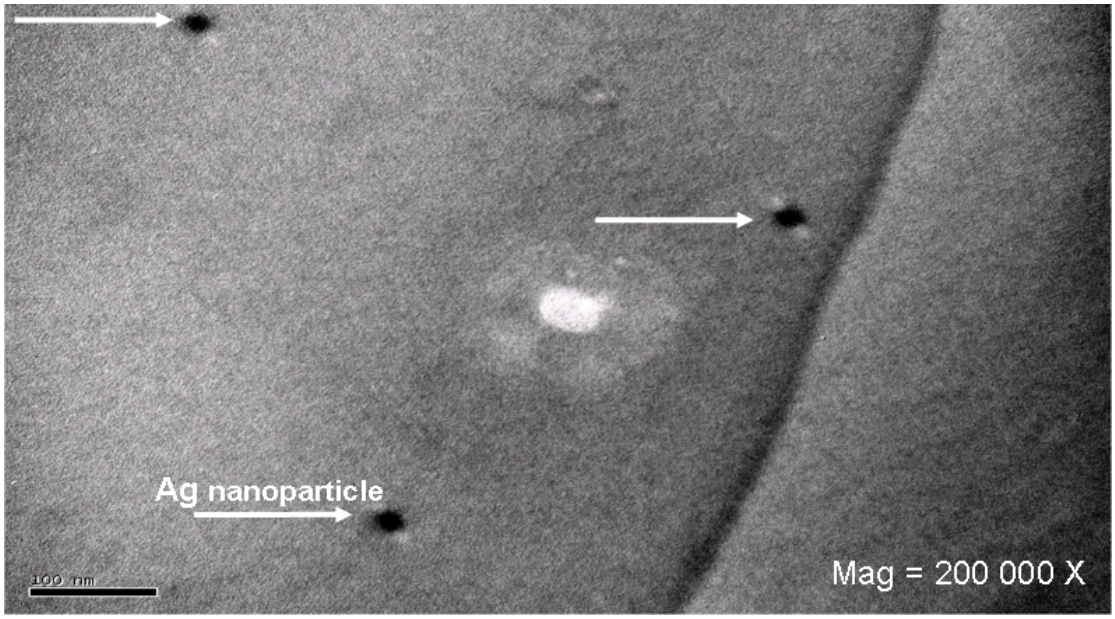

Figure 5. TEM image of silver nanoparticles stabilised with PVA. Colloidal dispersion was prepared as in Figure 1 and then diluted by a factor of 10 with methanol. The average diameter of nanoparticles were 21 – 22 nm, was determined using Image J.

diameter of the nanoparticles was determined to be in the range of 21 – 22 nm, using ImageJ software [37] which is in agreement with the DLS result.

X-Ray Diffraction, XRD.

X-ray diffraction (XRD) analysis was conducted on the drop coated Ag/polymer nanocomposite on a glass substrate. A number of strong Bragg reflections were observed which correspond to the (111 - ~ 39^{o}), (200 - ~ 45^{o}), (220 – ~ 66^{o}), (311 – ~ 79^{o}) reflections of face centred cubic silver [38 - 41], figure 6, indicating that the silver nanoparticles within the coating are crystalline. It should be noted that the peak at ~ 48^{o} can be attributed to the presence of sodium [42] as a result of the synthesis process.

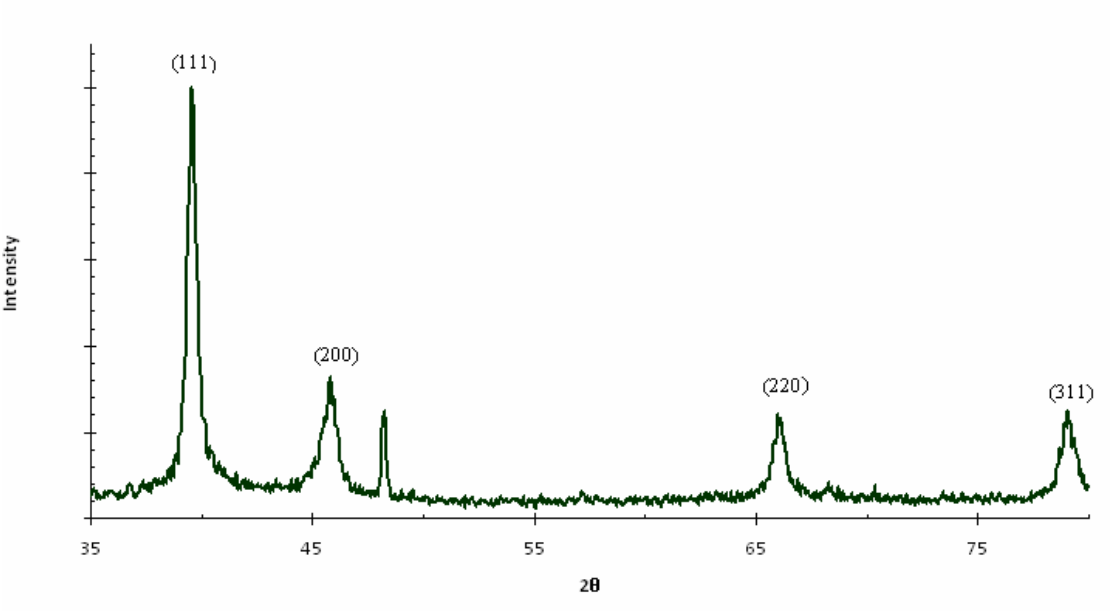

Figure 6. XRD pattern recorded from a drop-coated film of Ag/polymer nanocomposite on glass substrate.

Humidity measurements.

A clear response was observed when the coated substrates were exposed to water vapour. This response was found to be both rapid and repeatable over time. Figure 7 shows the sensor's response to repeated exposures at regular time intervals; the response is immediate, with a relatively consistent maximum peak height, with a total response time (despite a slight lag in the decay of the response signal) observed of 5 - 10 seconds.

Early results indicated that the coatings possessed a relatively good selectivity as a humidity detector. Vapour streams were produced by bubbling N_2 through the appropriate solvent contained in an insulated Dreschel flask, (Figure 2), in order to maintain a constant temperature and thus vapour pressure/concentration. A clear response for water vapour was observed with no obvious response for other non-polar vapours such as cyclohexane, as shown in Figures 8 and 9 and summarised in Table 1. It can be seen from Figures 8 and 9 and Table 1 that there is a dramatic difference in response between water and a quite polar vapour, methanol. On magnification of the response (Figure 9) there is a small peak due to methanol and acetonitrile. However, these peaks are significantly smaller than those that would have been expected on the basis of their dielectric constants.

An investigation was conducted by placing the coated interdigital electrode in a precisely controlled environment chamber with a humidity control system. Here the sensor's response to increasing % RH at a constant temperature of 21.3 ± 0.1^{o}C was found to be constant and relatively linear over the 10-60% RH range. Before each measurement, the sensor was 'powered off' i.e. no voltage was applied across it and the environment set to the % RH of interest. Before each reading, the environment was allowed to equilibrate for 30 mins. Figure 10 shows the steady state response obtained in this analysis. In this case, the humidity levels being measured were already constant before 'sensing' occurred, resulting in a response with none of the ramping up or down seen previously in Figures 7 and 8 where the amount of water vapour was altered during the measurement.

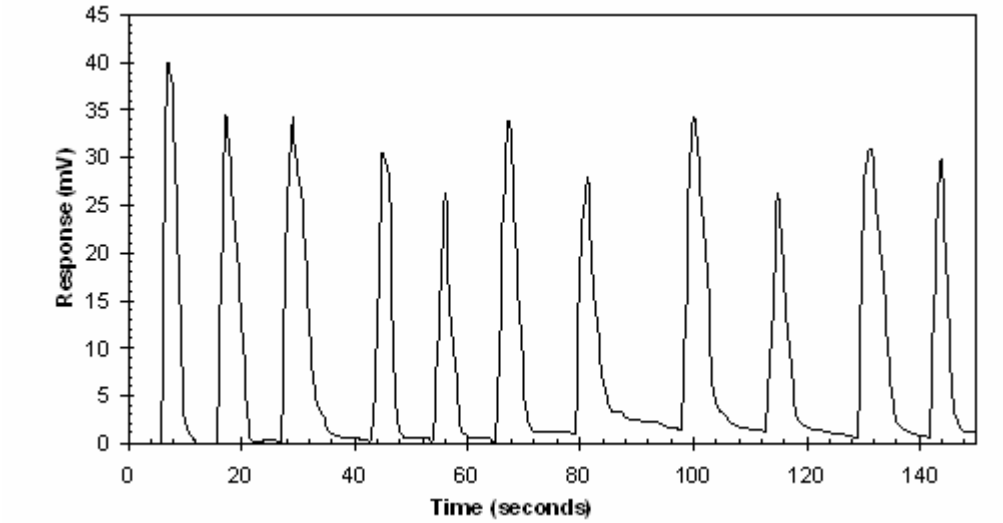

Figure 7. Representative plot of sensor's response to a change in environment. The sensing membrane was repeatedly exposed to water vapour at regular time intervals. (1mV=1μA)

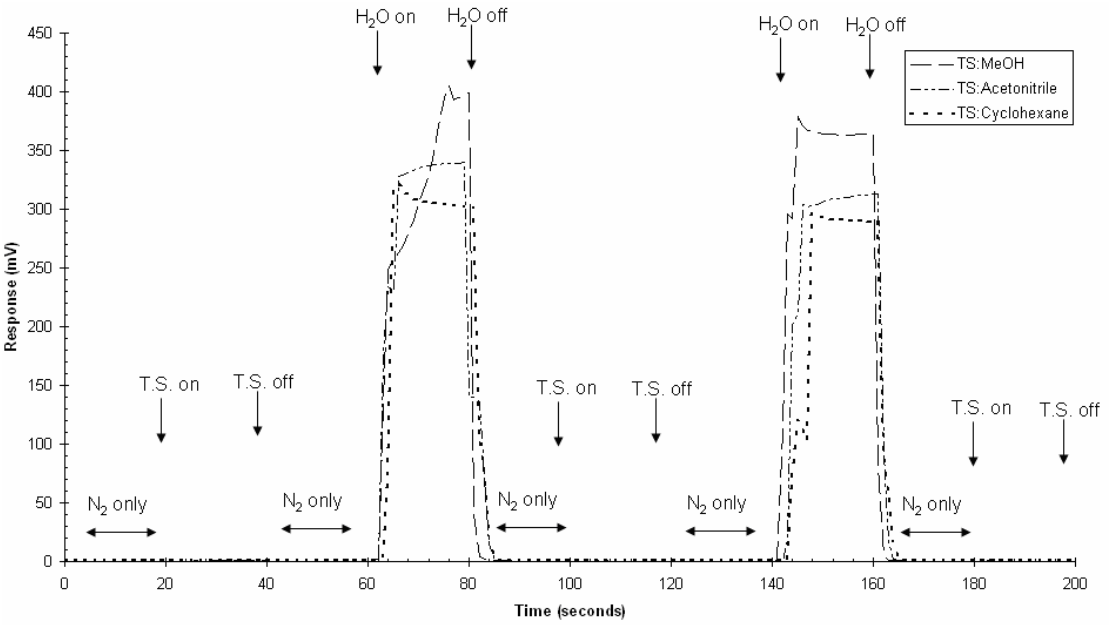

Figure 8. Sensor's response to exposure to various solvent vapours, summarised in Table 1. Exposure was conducted using the bubbler apparatus, where the streams passing over the sensing membrane were 'switched' from the reference gas to either the test solvent (T.S.) or water vapour as indicated.

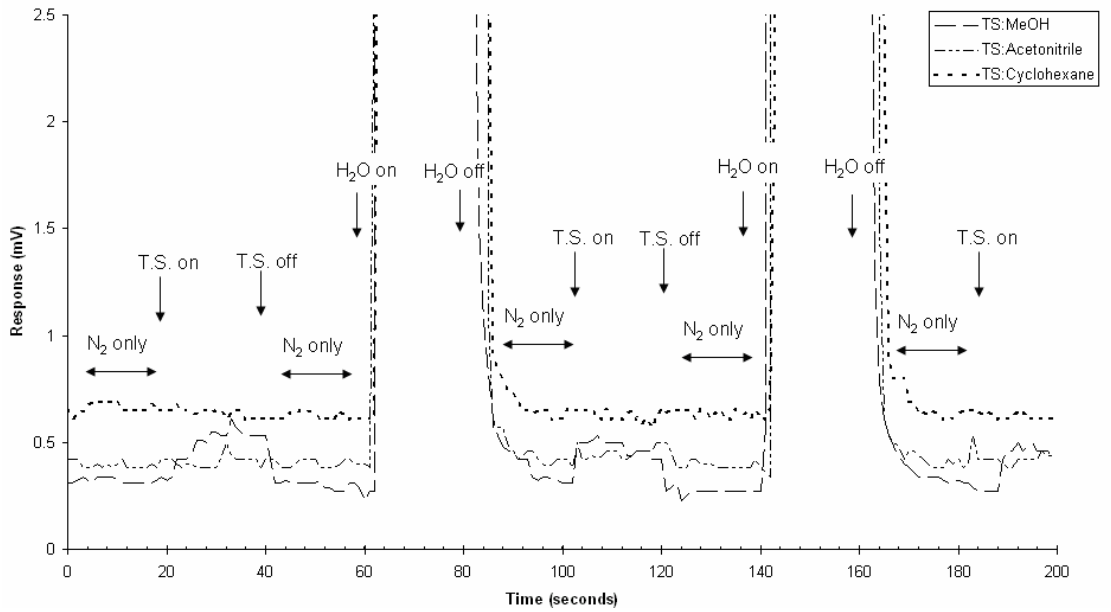

Figure 9. Magnification of the sensor's base line response of the results displayed in figure 8, illustrating the negligible response of certain test solvent (T.S.) vapours.

Vapour	B.P. at 1 Bar (^{o}C)	Dielectric constant at 20^{o}C	Response
Water	100	80.4 [43 a]	Yes
Acetonitrile	81	37.5 [43 b]	Negligible
Methanol	68	32.6 [43 c]	Negligible
Ethanol	78	24.3 [43 d]	Negligible
Cyclohexane	80.7	2 [43e]	No

Table 1. Summary of sensor's response during exposure to different vapours. All vapour solvents were maintained at 30^{o}C.

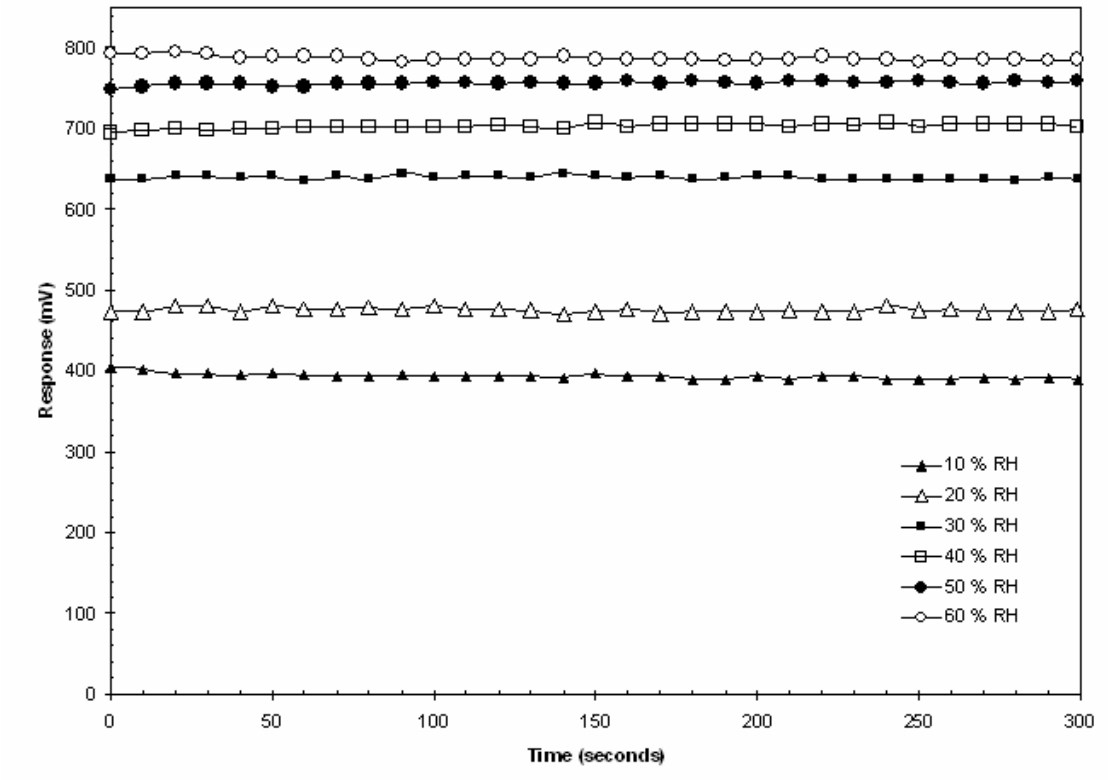

Figure 10. Graphical representation of sensor's response to increasing % RH over time at a constant temperature of 23.1^{o}C.

Typical results for repeated exposures of the same film (exposed repeatedly to set % RH humidities in the 10 – 60 % RH range) are summarised in Figure 11. It is thought

that the mechanism of the sensing layer in this study may involve the presence of electrolyte remaining from the synthesis in the polymer. Introduction of water vapour allows hydration of the electrolyte, increasing its mobility which allows an increase in current. It should be noted if the values of the responses for each % RH in Figure 11 were plotted; the resulting line would be relatively linear. However it would produce a positive intercept, as prior analysis indicated that at 0 % RH, no response occurred the sensor's response was modelled with a Langmuir adsorption equation [38], both first and second order, eqn (3) and (4) respectively. The second order model was observed to be the best fit as indicated in Figure 11 by the broken lines.

$$\mathbf{S = S/Ss\ (K_bC/\ (1+\ K_bC))} \qquad \mathbf{(3)}$$

$$\mathbf{S = S/Ss\ (Kb\sqrt{C}/\ (1+\ K_b\sqrt{C}))} \qquad \mathbf{(4)}$$

Where the fit parameters K_b and S_S are the binding constant and the relative signal at saturation and C is the relative the % RH [44].

In Figure 12, the responses of four different sensing layers at incremental levels of humidity at the 100 second measurement time are compared graphically.

It should be noted that variations were observed for different sensors (same coating on similar substrates). This variation may be attributed to the composition of the sensing layer in each case, particularly in terms of the coatings thickness. Preliminary results with the Reichert-Jung optical microscope indicated that the coatings ranged from 10μm -15μm. As the sensing layer conductivity increases with greater analyte levels and since the film contains ions, the observed response was initially thought to be due to ionic movement. In order to determine the role of silver nanoparticles (if any), a similar composite of the same ionic strength was prepared (using $NaNO_3$ instead of $AgNO_3$) which yielded no response to any of the analytes investigated under the same experimental conditions. This suggests that the suspected migration of anions in the composite on exposure to water vapour is not the sole sensing mechanism.

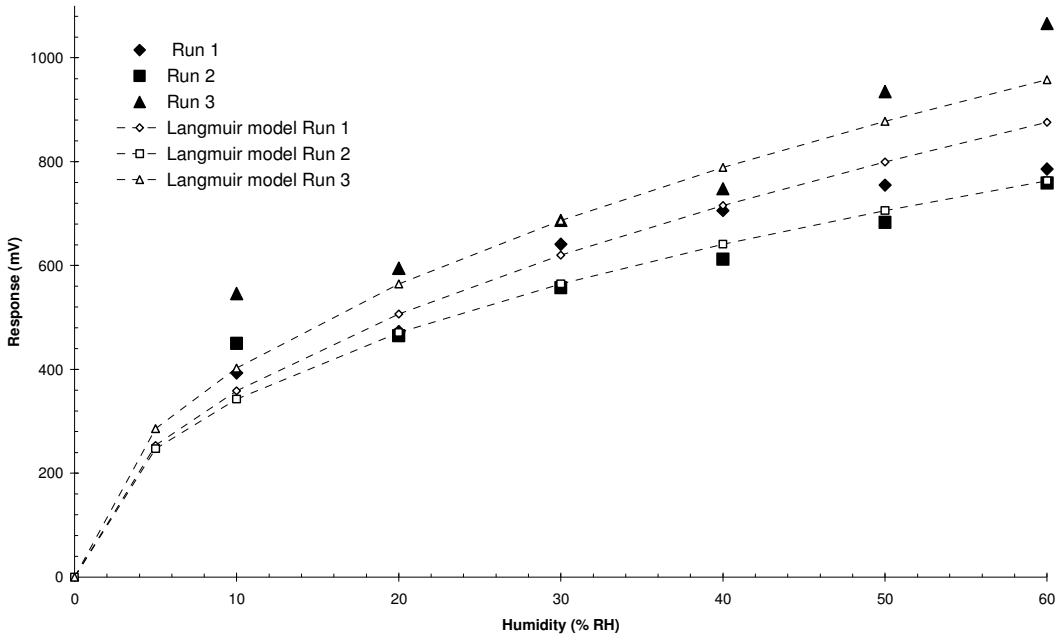

Figure 11. The sensor's response to repeated exposures to varying % RH at set time intervals. The dotted lines are the Langmuir model of the experimental data according to second order kinetics (equation 4).

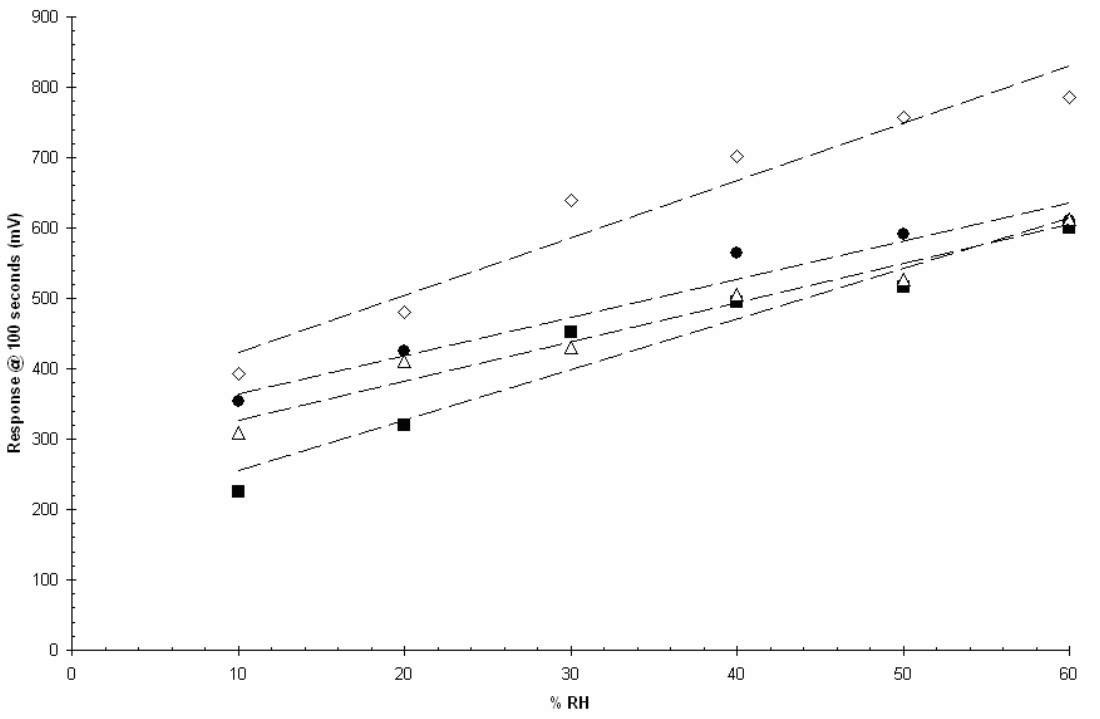

Figure 12. Responses of four different sensors prepared separately. The slopes for the lines are 5.4, 5.5, 7.2 and 8.2 (mV/%RH).

However, layer thickness is not yet well defined using the drop casting process resulting in a significant variation in coating thickness which can be assumed to have an impact on the reproducibility of the sensitivity for each layer as seen in Figure 11, thus more work is required to optimise the thickness of the coating.

Cyclic Voltammetry

The cyclic-voltammetry study of the cast film on the interdigits, (2 electrode system), indicated that the sensor coating appears to act as a background electrolyte in the presence of water vapour. No sensor response (i.e. current) was observed when the coating was exposed in the N_2 vapour stream. However while the film displays a clear electrochemical response in a higher humidity environment, (where there was an anodic peak that was attributed to Ag oxidation and a cathodic peak corresponding to Ag^+ reduction.) in the resulting voltammograms, both the silver nanoparticles and the ions within the coating appear to have an active role in the sensor's mechanism.

Analysis of a typical voltammogram indicated that approximately $6x10^{-10}$mols of silver within the coating undergoes oxidation and reduction; a fraction (~1/10,000) of the molar silver content of the cast nanocomposite coating. This may explain why, although the sensors observed response appears to be migration controlled, no drop off of the steady state signal is observed during prolonged periods of exposure.

Electrochemical Impedance Spectroscopy, EIS.

Impedance measurements were carried out over the frequency range of 1 Hz - 1 MHz using a Solartron Electrochemical Interface, SI 1287 and a Solartron 1255B Frequency Response Analyser. Humidity levels were established using closed vessel humidity saturated salt solutions, potassium acetate for 20%, calcium chloride 35% and calcium nitrate 55% [45]. For each humidity level before the response was measured the sensor was placed in the relevant sealed container and left overnight to equilibrate. All measurements were carried out at a constant temperature of $20 \pm 2\ ^oC$. Figures 13 and 14, show typical (multiple measurements were conducted) electrochemical impedance spectra of the sensing coating at different the humidity levels, Nyquist and Bode respectively.

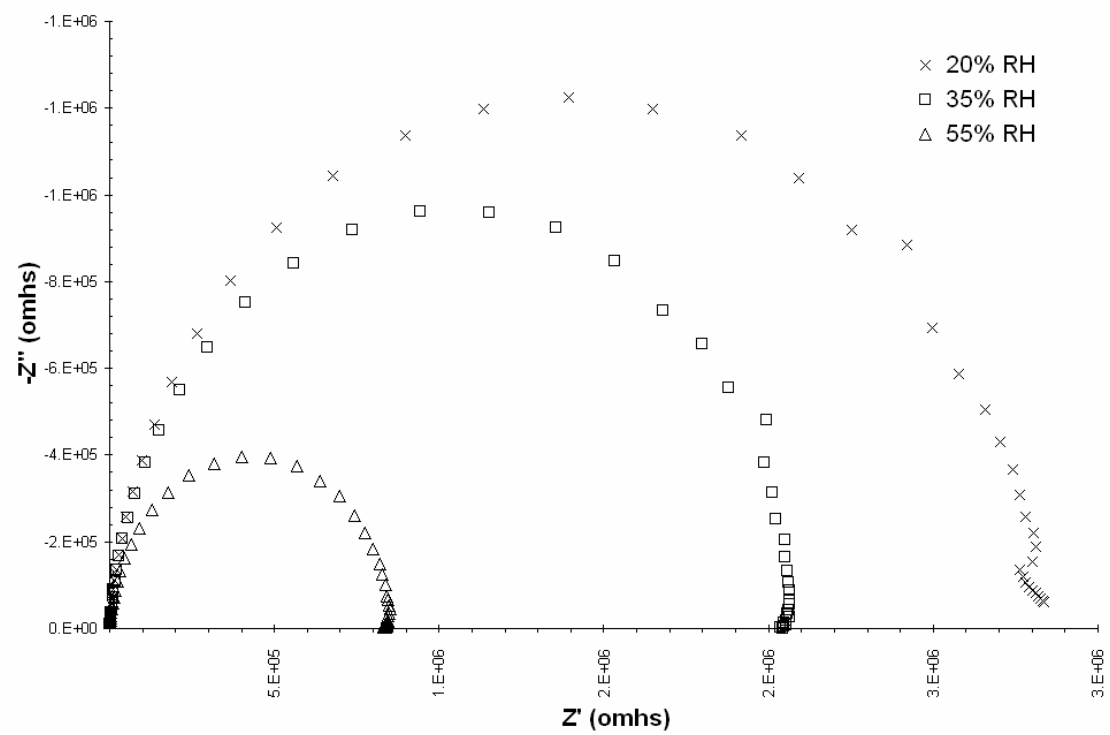

Figure 13. Nyquist plot of effect of humidity on the impedance of the sensing coating.

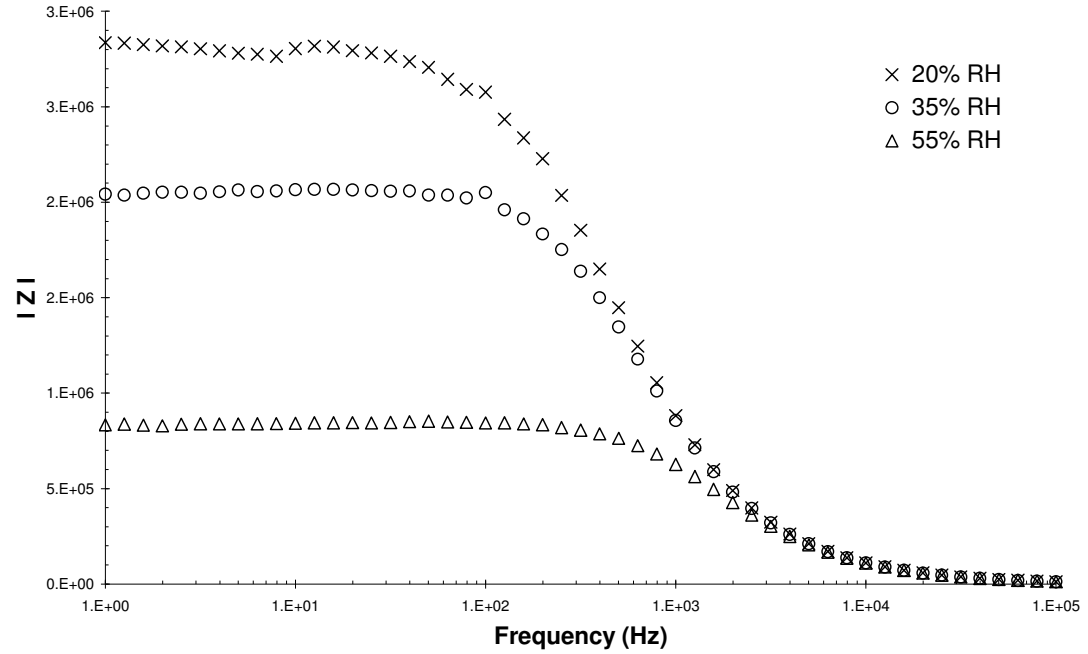

Figure 14. Bode plot of effect of humidity on the impedance of the sensing coating.

It can be seen that an increase in humidity results in a decrease of the sensing film's impedance. The EIS spectra of the coating at each humidity level can be fitted to a modified Randles circuit figure 15, the results of which are tabulated in table 2. Modelling was conducted using Z view 2 software.

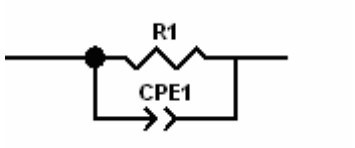

Figure 15. Modified Randles Circuit Model.

Element	Modelled Value	% Error
20% RH		
Resistor	2.80 x 10^{6} Ω	0.269
CPE-T	2.94 x 10^{-10} F	1.252
CPE-P	0.935	0.126
35% RH		
Resistor	2.08 x 10^{6} Ω	0.146
CPE-T	2.61 x 10^{-10} F	0.748
CPE-P	0.946	0.073
55% RH		
Resistor	8.48 x 10^{5} Ω	0.135
CPE-T	2.50 x 10^{-10} F	0.932
CPE-P	0.949	0.088

Table 2. Summary of sensor's modelled response during EIS at different %RH levels.

Sensing mechanism.

The precise mechanism of the process is still unclear, although the necessity of silver nanoparticles within the sensor was confirmed by comparing the response of a coating with no silver but of the same ionic strength. This was achieved by the replacement of $AgNO_3$ with $NaNO_3$ in the coating synthesis. The coating containing no silver showed no response to changing humidity levels. One possible mechanism could be a form of ionic migration with the introduction of water vapour during exposure hydrating the electrolyte (a result of synthesis process) thereby enabling the movement of ions surrounding each nanoparticle, with the nanoparticles acting like a scaffold along which the current may flow. As the silver nanoparticles were found to have a negative zeta potential in solution, should they maintain a double layer in the cast film, exposure of the film to water vapour could allow hydration of ions enhancing their

mobility allowing the movement of ions from one nanoparticles double layer to the next.

Conclusions

Silver-polyvinyl alcohol colloidal dispersions were successfully prepared by the reduction of aqueous $AgNO_3$ with $NaBH_4$ using PVA as a capping agent. The stoichiometric molar ratio of $AgNO_3$:$NaBH_4$ was determined as 1:1. The effect of temperature on the preparation process was observed to be important with lower temperatures (< 4^oC) resulting in the production of colloids with greater nanoparticle content. Preparation of the colloids at low temperatures also had a positive effect with the reduction of the particle size range in the colloids, which was verified by UV-Vis spectroscopy and Dynamic Light Scattering.

DLS analysis determined the particle size range to be 8nm – 38nm (with an average of 21-22 nm) in the colloids, which correlated well with the findings of TEM analysis where silver nanoparticles were observed to have an average size of 22nm. The nanoparticle composite when cast on an interdigital electrode array and on application of a constant potential was observed to produce a current, which was proportional to levels of humidity from 10% RH to 60% RH. The sensor gave a reversible rapid response at standard temperature and pressure. The steady state response was selective and increased with increasing levels of humidity.

Acknowledgements

A.C. Power thanks the ABBEST PhD Scholarship Programme of the Dublin Institute of Technology, and everybody in the FOCAS Institute/DIT for their assistance during the experimental work.

References

[1]. Z. Yan, M.J. Sousa-Gallagher; F.A.R Oliveira, J. Food Eng., 2008, 84, 359–367.

[2]. Singh, R.P. Shelf life evaluation of foods, Man, C.M.D.; Jones, A.A. Ed.s, Blackie Academic & Professional, Glasgow, (1992) 3–24.

[3]. E.L.J. Goossens, A.J.J. van der Zanden, W.H. van der Spoel, Prog. Org. Coat., 2004, 49, 270–274.

[4]. B. Adhikari, S. Majumdar, Prog. Polym. Sci., 2004, 29, 699–766.

[5]. H. Bai, G.Q. Shi, Sensors, 2007, 7, 267-307.

[6]. C.Y. Lee, G.B. Lee, Sensor Letters, 2005, 3, 1-15.

[7]. L. Han, X. Shi, W. Wu, F.L. Kirk, J. Luo, L. Wang, D. Mott, L. Cousineau, S.I. Lim, S. Lu, C.J. Zhong, Sens. Actuators, B, 2005, 106, 431-441.

[8]. X. Luo, A. Morrin, A.J. Killard, M.R Smyth, Electroanalysis, 2006 18, 319-326.

[9]. I. Naydenova, R. Jallapuram, V. Toal, S. Martin, Appl. Phys. Lett., 2008, 92, DOI 031109.

[10]. C. Drake, S. Deshpande, D. Bera, S. Seal, Int. Mater. Rev., 2007, 52, 289-317.

[11]. E. Katz, I. Willner, J. Wang, Electroanalysis, 2004, 16, 19-44.

[12]. J.H. Lee, Sens. Actuators, B, 2009, 140, 319–336.

[13]. U. Lange, N.V.. Roznyatovskaya, V.M. Mirsky, Anal. Chim. Acta.,2008, 614, 1–26.

[14]. A. Pron, P. Rannou, Prog. Polym. Sci., 2002, 27, 135-190.

[15]. Y. Li, M.J. Yang, Y. She, Talanta, 2004, 62, 707-712.

[16]. A. Walcarius, D. Mandler, J.A. Cox, M. Collinson, O.J. Lev, Mater. Chem., 2005, 15, 3663-3689.

[17]. B. Adhikari, S. Majumdar, Prog. Polym. Sci., 2004, 29, 699-766.

[18]. R. Tarushee Ahuja, D. Kumar, Sens. Actuators, B, 2009, 136, 275–286.

[19]. Z. M. Rittersma, Sens. Actuators, A, 2002, 96, 196-210.

[20]. D. D. Perrin, W.L.F. Armarego, Purification of laboratory chemicals 3rd ed., Pergamon, Oxford, (1988)

[21]. M. Bernabò, A, Pucci, H, Harimino, R, Giacomo, Materials, 2010, DOI: 10.3390/ma3021461

[22]. N.R. Jana, L. Gearheart, C.J. Murphy, Chem. Commun. 2001, 7, 617–618

[23]. S.D. Solomon, M. Bahadory, A.V. Jeyarajasingam, S.A. Rutkowsky, C. Boritz, L. Mulfinger,. J. Chem. Educ. 2007, 84, 322–325.

[24]. Q.F . Zhou, J.C. Bao, J. Xu,. J. Mater. Chem., 2002, 12, 384-387.

[25]. Y.J. Yang, Mater. Sci. Eng., B, 2006, 131, 200–202.

[26]. V.K. Sharma, R.A.. Yngard, Y. Lin, Adv. Colloid Interface Sci., 2009, 145, 83–96.

[27]. Z.H. Mbhele, M.G. Salemane, C.G.C.E. van Sittert, J.M. Nedeljkovic, V. Djokovic, A.S. Luyt, Chem. Mater., 2003, 15, 5019-5024.

[28]. P.K. Khanna, N. Singh, S. Charan, V.V.V.S. Subbarao, R. Gokhale, U.P. Mulik, Mater. Chem. Phys., 2005, 93, 117-121.

[29]. www.bvt.cz/_files/438/cc2.pdf (last accessed April 2010)

[30]. T. Li, H.G. Park, S. Choi, Mater. Chem. Phys., 2007, 105, 325-330.

[31]. K.L. Kelly, E. Coronado, L.L. Zhao, G.C. Schatz, J. Phys. Chem. B, 2003, 107, 668-677.

[32]. C.F. Bohren, D.R. Huffman, Absorption and scattering of light by small particles, New York; Chichester: Wiley, (1983)

[33]. Y. Kunieda, K. Nagashima, N. Hasegawa, Y. Ochi, Spectrochim. Acta, Part B, 2009, 64, 744–746.

[34]. E. Filippo, A. Serra, D. Manno, Sens. Actuators, B, 2009, 138, 625–630.

[35]. W. Likussar, D.F. Boltz, Anal. Chem., 1971, 43, 1265–1272.

[36]. P. Atkins, J. de Paula, Atkins' Physical Chemistry, 7th ed., Oxford University Press, Oxford; New York, (2002), 845.

[37]. http://rsb.info.nih.gov/ij/ (Downloaded May 2009)

[38]. A. Sinha, B. P. Sharma, Bull. Mater. Sci., 2005, 28, 3, 213–217

[39]. S. Mandal, S. K. Arumugam, R. Pasricha M. Sastry, Bull. Mater. Sci., 2005, 28, 503–510

[40]. D.G. Yu, W.C. Lin, C.H. Lin, L.M. Chang, M.C. Yang, Materials Chemistry and Physics 2007, 101, 93–98

[41]. W.C. Lin, M.C. Yang Macromol. Rapid Commun. 2005, 26, 1942–1947

[42]. F. Guo, Z.G. Peng, J.Y. Dai, Z.L. Xiu, Fuel Processing Technology, 2010, 91, 322–328

[43 a-e]. CRC Handbook of Chemistry and Physics, D.R. Lide, Editor in chief, 89th ed., Boca Raton, Fla, CRC; London, Taylor & Francis, (2008)

[a] pp 6-163.

[b] pp 8-138.

[c] pp 8-140.

[d] pp 8-139.

[e] pp. 8-136

[44]. Y. Joseph, B. Guse, A. Yasuda, T. Vossmeyer, Sens. Actuators, B, 2004, 98, 188-195.

[45]. CRC Handbook of Chemistry and Physics, D.R. Lide, Editor in chief, 89th ed., Boca Raton, Fla, CRC; London, Taylor & Francis, (2008), 15-33 - 15-34